An innovative satellite sunlight-reflection staring attitude control

Fuzhen Zhang [1] and Lei Jin[2]
School of Astronautics, Beihang University, 100191 Beijing, China.

Gustavo Alonso Rodrigo[3]
Instituto Universitario de Microgravedad Ignacio Da Riva (IDR/UPM),

Universidad Politécnica de Madrid, 28040 Madrid, Spain.

A so-called sunlight-reflection staring control for spacecraft on low Earth orbit is discussed such that the sunlight, reflected by an on-board reflector, will point to a target point on Earth surface during a short period of time. The new method begins with the establishment of the target reference frame, whose attitude quaternion, angular velocity and acceleration are calculated afterwards. The "PD+" control technique is adopted to achieve the attitude tracking. Moreover, the conditions under which the sunlight-reflection staring is analyzed, and the geographic information of the actual staring point are computed to analyze the accuracy of the method. The simulation section results validate the control performance.

I. Introduction

Staring attitude control has been increasingly introduced along the last decades through the development of the space technology. In general, staring attitude control can be summarized saying that a vector fixed on the spacecraft will remain parallel to a different desired vector fixed on another reference frame. For example, for some Earth observation satellites in low-Earth orbit (LEO) with a camera, the staring attitude control

[1] PhD Student, School of Astronautics, Beihang University, Haidian District, 100191 Beijing, China.
[2] Associate Professor (Corresponding author), School of Astronautics, Beihang University, Haidian District, 100191 Beijing, China. Email: jinleibuaa@163.com
[3] Professor, Instituto Universitario de Microgravedad Ignacio Da Riva (IDR/UPM), Universidad Politécnica de Madrid, 28040 Madrid, Spain.

mode can help to monitor a location of interest on Earth continuously to deal with emergencies, such as fire disasters, explosions, earthquakes and so on, by providing real-time video images with high resolution for the target location.

To the authors' best knowledge, DLR-TUBSAT, launched in 1999, is the first reported small satellite with target pointing ability, which can also send video images to the ground [1, 2]. For this satellite, interactive attitude control was implemented via the keyboard or mouse, which steered the pointing direction of the camera platform to the interesting event [2]. Later, the LAPAN-TUBSAT was launched in 2007 with an interactive attitude control [3]. Due to the man-in-loop system of these two satellites, no effective control algorithm to achieve the ground point tracking was adopted. A control strategy is proposed in [4] such that the attitude tracking to point to a fixed point on Earth surface can be achieved automatically. A target reference frame is established, whose attitude quaternion and angular velocity are given. However, in this problem, only the optical axis fixed to the spacecraft is required to point to the target point while no other constraints are specified. To accomplish the establishment of the target reference frame, additional constraints are required, such as the minimization of the angular rates[4], no relative rotation along optical axis [5, 6] or zero-yaw-angle[7]. A fuzzy-logic based controller is proposed in [5] where however, the Earth is assumed to be a sphere. Furthermore, a sliding mode control law is presented in [6] to observe a ground target location where a disturbance observer is designed. In [7], a numerical approach to compute the target angular rate is proposed, which is verified to be feasible in real practice. However, it does not clearly state how to calculate the optical axis according to the geographic information of the target.

In essence, the staring control can be treated as an attitude tracking problem. To deal with the uncertainties, the sliding mode control (SMC) [8–10], intelligent control[11–14] technique are usually applied. Furthermore, the fault tolerant control (FTC) is usually utilized to deal with the unexpected actuator faults or failures [15–17]. The control strategies in the aforementioned studies can guarantee a good tracking performance and strong disturbance rejection capability, which however, require a large control torque. Comparatively speaking, PD or "PD+" type controller have a wider application in real practice for the attitude control system. Compare to PD, an additional feed-forward item is included in the "PD+" controller to compensate some known but ignored influence. The asymptotical stability of the attitude tracking problem with a "PD+" controller is analyzed in [18] based on Matrosovs theorem and Barbalat's Lemma, in the framework

of Modified Rodrigues Parameters (MRPs).

Sometimes, we may need sunlight to point to the target point on ground through the reflection of the spacecraft. A recent example is the Russian Mayak Cubesat, launched in July 2017, which became one of the brightest objects in sky by reflecting the sunlight with the on-board solar reflector. Motivated by this, we aim to achieve an attitude control such that the sunlight, reflected by the spacecraft, can point to a fixed point on Earth ground at any instant during the process, which is the so-called sunlight-reflection staring mode. Similar to the traditional staring mode control, as previously mentioned, the reflected sunlight can be regarded as the optical axis, which however, is no longer body-fixed. Furthermore, in some existed literatures [4–7], it is assumed that the vector from the satellite to the target point is known, which however is not practical. Instead, usually only the latitude and longitude information are given in practice. Conversely, we may be concerned about the latitude and longitude of the staring point to analyze the effectiveness and precision of the control law, which is not presented in those references.

To overcome these shortages, we propose a sunlight-reflection staring control method such that the reflected sunlight will point to the target ground location, specified by the geographic latitude and longitude with the following contributions: 1) It is assumed that the Earth is an ellipsoid instead of a sphere. 2) A simple and practical method to calculate target angular rate and acceleration will be shown, so that a "PD+" control law can be adopted. 3) We will also analyze when the sunlight-reflection staring mode can be achieved and how to calculate the geographic latitude and longitude of the actual staring point.

This paper is arranged as follows. In Section II, the dynamics of a rigid spacecraft are described. Then in Section III, the target reference frame is established. In what follows of this section, the target quaternion, angular rate and angular acceleration are computed according to the geographic information of the selected target point. Also, we will present an analysis about the condition when the control mode can be achieved and how to calculate the actual staring point. In Section IV, a "PD+" type controller is designed. The numerical simulation is conducted in Section V to verify the effectiveness of the proposed method followed by the Conclusions section.

II. Preliminaries

In this paper, we define that, for a given $\boldsymbol{x} \in \mathbb{R}^n$ and $\boldsymbol{A} \in \mathbb{R}^{m\times n}$ and reference frame $\boldsymbol{F}_B$, ${}^B\boldsymbol{x}$ represents the vector $\boldsymbol{x}$ described in reference $\boldsymbol{F}_B$. $\boldsymbol{A}^T$ denotes the transposed matrix of $\boldsymbol{A}$. $\boldsymbol{E}_n$ denotes the n-dimensional identity matrix. $\|\boldsymbol{x}\| = \sqrt{\boldsymbol{x}^T\boldsymbol{x}}$ denotes the Euclidean norm of the vector $\boldsymbol{x}$. $< \boldsymbol{a}, \boldsymbol{b} >= \arccos(\frac{\boldsymbol{a}\cdot\boldsymbol{b}}{\|\boldsymbol{a}\|\|\boldsymbol{b}\|})$ denotes the angle of the vectors $\boldsymbol{a}$ and $\boldsymbol{b}$. Furthermore, given $\boldsymbol{x} = [x_1\ x_2\ x_3]^T, \boldsymbol{y} = [y_1\ y_2\ y_3]^T \in \mathbb{R}^3$, $\boldsymbol{x}\cdot\boldsymbol{y} = \boldsymbol{x}^T\boldsymbol{y}$ and $\boldsymbol{x}\times\boldsymbol{y} = \boldsymbol{x}^\times\boldsymbol{y}$ where

$$\boldsymbol{x}^\times = \begin{bmatrix} 0 & -x_3 & x_2 \\ x_3 & 0 & -x_1 \\ -x_2 & x_1 & 0 \end{bmatrix}$$

.

A. The definitions of the reference frames

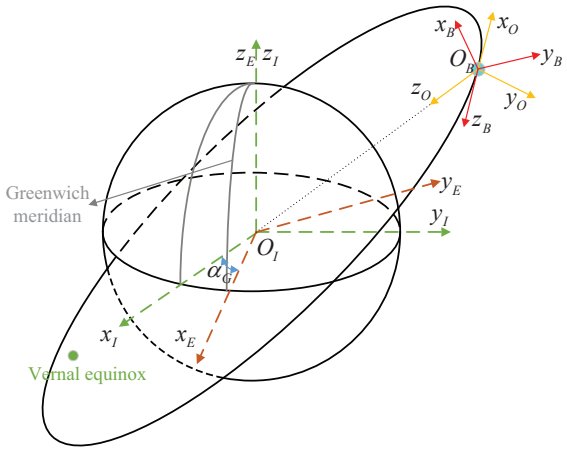

Fig. 1 The definitions of the corresponding reference frames

The attitude is defined to describe the relative orientation of the spacecraft with respect to another reference frame. Some reference frames are defined firstly as is in Fig.1.

Earth-center Inertial Reference Frame (ECIRF, $\boldsymbol{F}_I(O_I x_I y_I z_I)$): The origin O_I of the ECIRF is fixed to the Earth center. The z_I-axis lies along the direction of the Earth rotation axis and x_I-axis lies on the equatorial plane, pointing to the vernal equinox of the time J2000. The y_I-axis lies in the equatorial plane completing the right-hand orthogonal reference.

Orbital Reference Frame (ORF, $\boldsymbol{F}_O(O_o x_o y_o z_o)$): The z_o-axis lies in the orbital plane pointing to the

Earth center while the origin O_o lies on the mass center of the spacecraft. x_o-axis lies on the orbital plane, along the direction of the velocity of the spacecraft and the y_o-axis is perpendicular to the orbital plane completing the right-hand orthogonal reference.

Earth Reference Frame (ERF, $\boldsymbol{F}_E(O_E x_E y_E z_E)$): The origin O_E of ERF is fixed to the Earth center. The z_E-axis coincides with z_I and x_E-axis lies along the intersection line of the equatorial plane and the Greenwich meridian plane. y_E lies on the equatorial plane completing the right-hand orthogonal references.

Body Reference Frame (BRF, $\boldsymbol{F}_B(O_B x_B y_B z_B)$): The origin O_B of the BRF is in the mass center of the spacecraft and the three axes are aligned with the principal axes of inertia.

B. Spacecraft attitude dynamics and kinematics

Consider a rigid spacecraft with the following dynamics formulation:

$$\boldsymbol{I}_b \, {}^B\dot{\boldsymbol{\omega}}_{BI} + {}^B\boldsymbol{\omega}_{BI}^{\times} \boldsymbol{I}_b \, {}^B\boldsymbol{\omega}_{BI} = \boldsymbol{T}_c \tag{1}$$

where symmetrical positive definite matrix $\boldsymbol{I}_b \in \mathbb{R}^{3\times3}$ denotes the inertia matrix of the spacecraft. ${}^B\boldsymbol{\omega}_{BI} \in \mathbb{R}^3$ is the angular rate vector of the spacecraft with respect to $\boldsymbol{F}_I$ and described in the $\boldsymbol{F}_B$. $\boldsymbol{T}_c \in \mathbb{R}^3$ is the control torque about the body axes.

The relative orientation of the spacecraft ($\boldsymbol{F}_B$) with respect to $\boldsymbol{F}_I$ can be described in the form of unit quaternions, which follows that:

$$\begin{cases} \dot{\bar{q}}_{BI} = -\frac{1}{2} \hat{\boldsymbol{q}}_{BI}^T \, {}^B\boldsymbol{\omega}_{BI} \\ \dot{\hat{\boldsymbol{q}}}_{BI} = \frac{1}{2} \left(\bar{q}_{BI} \boldsymbol{E}_3 + \hat{\boldsymbol{q}}_{BI}^{\times} \right) {}^B\boldsymbol{\omega}_{BI} \end{cases} \tag{2}$$

where $\boldsymbol{q}_{BI} = \left[\bar{q}_{BI} \ \hat{\boldsymbol{q}}_{BI}^T \right]^T \in \mathbb{R}\times\mathbb{R}^3$ represents the quaternion of the spacecraft satisfying that $\bar{q}_{BI}^2 + \hat{\boldsymbol{q}}_{BI}^T \hat{\boldsymbol{q}}_{BI} = 1$. Eqs.(1) and (2) describe the relative rotation model of the spacecraft with respect to $\boldsymbol{F}_I$.

Through simple calculation, it can be obtained that the rotation matrix from the $\boldsymbol{F}_I$ to $\boldsymbol{F}_B$ can be given by [19]

$$\boldsymbol{R}_{BI} = \left(\bar{q}_{BI}^2 - \hat{\boldsymbol{q}}_{BI}^T \hat{\boldsymbol{q}}_{BI} \right) \boldsymbol{E}_3 + 2\hat{\boldsymbol{q}}_{BI} \hat{\boldsymbol{q}}_{BI}^T - 2\bar{q}_{BI} \hat{\boldsymbol{q}}_{BI}^{\times} \tag{3}$$

C. Definitions and lemmas

Definition 1 *For the unit quaternions* $\boldsymbol{q}_1 = \left[\bar{q}_1 \ \hat{\boldsymbol{q}}_1^T\right]^T$ *and* $\boldsymbol{q}_2 = \left[\bar{q}_2 \ \hat{\boldsymbol{q}}_2^T\right]^T$*, the multiplicative operator* $\otimes$ *and the adjoint operator* $\boldsymbol{q}_1^*$ *are defined by*

$$\boldsymbol{q}_1 \otimes \boldsymbol{q}_2 = \left[\bar{q}_1\bar{q}_2 - \hat{\boldsymbol{q}}_1^T\hat{\boldsymbol{q}}_1 \ \ (\bar{q}_1\hat{\boldsymbol{q}}_2 + \bar{q}_1\hat{\boldsymbol{q}}_2 + \hat{\boldsymbol{q}}_1 \times \hat{\boldsymbol{q}}_2)^T\right]^T \tag{4}$$

$$\boldsymbol{q}_1^* = \left[\bar{q}_1 \ \ -\hat{\boldsymbol{q}}_1^T\right]^T \tag{5}$$

Lemma 1 *For* $\forall \boldsymbol{x}, \boldsymbol{y}, \boldsymbol{z} \in \mathbb{R}^3$*, the equation* $\boldsymbol{x} \times (\boldsymbol{y} \times \boldsymbol{z}) = (\boldsymbol{x} \cdot \boldsymbol{z})\,\boldsymbol{y} - (\boldsymbol{x} \cdot \boldsymbol{y})\,\boldsymbol{z}$ *always holds.*

III. Target attitude calculation

The aim of this work is to ensure that the reflected sunlight will point to a target point fixed to the Earth surface by adjusting the attitude of the spacecraft when it is in an appropriate location of the orbit. Without loss of generality, we assume an on-board sunlight reflector aligned along z_b axis of the spacecraft to reflect the sunlight (Fig.2). $\boldsymbol{S}_{sun}$ is the unit Sun direction vector (Earth-Sun vector). To achieve the target, similar to [7], we will define a so-called Reflective Staring Target Reference Frame $\boldsymbol{F}_T(O_T x_T y_T z_T)$ (RSTRF) such that $\boldsymbol{F}_B$ will correspond to $\boldsymbol{F}_T$.

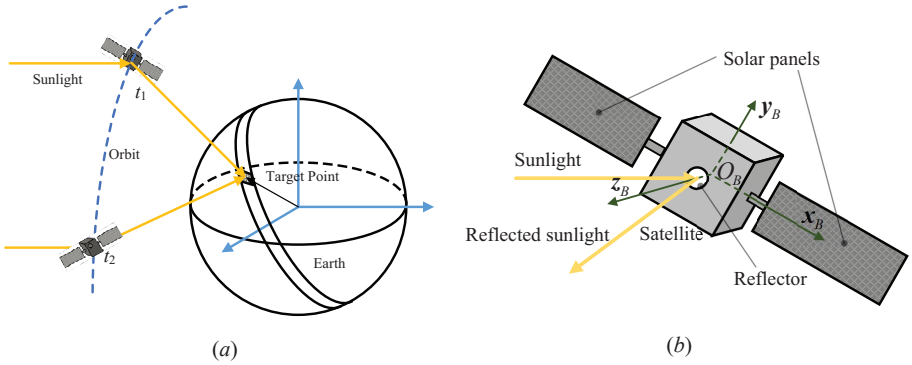

Fig. 2 The sunlight-reflected staring of the satellite

As in Fig.3, the target point on Earth surface is denoted by O_T. The vectors starting from the Earth center O_E to the satellite and the target points are denoted by $\boldsymbol{r}_s$, $\boldsymbol{r}_T$, respectively, and the vector from the satellite to the target point is denoted by $\boldsymbol{\rho}_T$. Thus, the three axes of $\boldsymbol{F}_T$ are defined as follows:

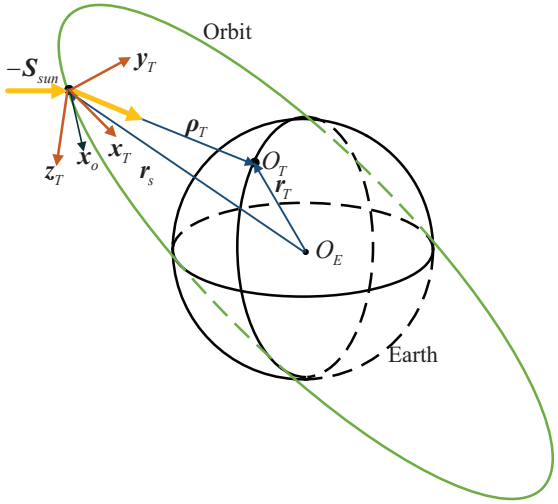

Fig. 3 The definition of the target reference frame

$$z_T = \frac{S_{sun} + \rho_T/\|\rho_T\|}{\|S_{sun} + \rho_T/\|\rho_T\|\|}, y_T = \frac{z_T \times x_o}{z_T \times x_o}, x_T = y_T \times z_T \tag{6}$$

where $\rho_T = r_T - r_s$ and $\rho_T/\|\rho_T\|$ represents the unit vector pointing to the target from the satellite.

A. Target quaternion

Three axes of F_T, according to Eq. 6, can be expressed in F_I as follows,

$$^I z_T = \frac{^I S_{sun} + ^I \rho_T/\|^I \rho_T\|}{\|^I S_{sun} + ^I \rho_T/\|^I \rho_T\|\|}, ^I y_T = \frac{^I z_T \times ^I x_o}{^I z_T \times ^I x_o}, ^I x_T = ^I y_T \times ^I z_T \tag{7}$$

and then the transform matrix from the F_I to F_T can be obtained as

$$R_{TI} = \begin{bmatrix} ^I x_T & ^I y_T & ^I z_T \end{bmatrix} \tag{8}$$

The Sun vector $^I S_{sun}$, is known by looking-up to the solar ephemeris. For $^I \rho_T$, it is clear that $^I \rho_T = ^I r_T - ^I r_s$. $^I r_s$ can be measured by the Navigation System or estimated by orbit prediction. The target point O_T on the Earth ground is usually given in the form of the geodetic latitude and longitude. Denote by Φ_T and Λ_T the geographical latitude and longitude of the target point O_T, and the vector r_T in F_E can be

described as [20, 21]

$$
{}^{E}\boldsymbol{r}_{T} = \begin{bmatrix} R_T \cos\Phi_T \cos\Lambda_T \\ R_T \cos\Phi_T \sin\Lambda_T \\ R_T \left(1 - e_E^2\right) \sin\Phi_T \end{bmatrix} \tag{9}
$$

where

$$
R_T = \frac{R_E}{\sqrt{1 - e_E^2 \sin^2\Phi_T}}
$$

is the radius of curvature and $R_E = 6\,378\,137\,\mathrm{m}$ is the semi-major axis (equatorial radius) of the Earth (Ellipsoid); $e_E = \sqrt{1-(1-f_E)^2}$ is the eccentricity of the Earth's profile and $f_E = 1/298.2572$ is the oblateness of the Earth. Thus,

$$
{}^{I}\boldsymbol{r}_{T} = \boldsymbol{R}_{IE}\,{}^{E}\boldsymbol{r}_{T} \tag{10}
$$

in which $\boldsymbol{R}_{IE}$ is the transform matrix from the Earth Reference Frame $\boldsymbol{F}_E$ to the Inertial Reference Frame $\boldsymbol{F}_I$, described by

$$
\boldsymbol{R}_{IE} = \begin{bmatrix} \cos\alpha_G & -\sin\alpha_G & 0 \\ \sin\alpha_G & \cos\alpha_G & 0 \\ 0 & 0 & 1 \end{bmatrix}
$$

where α_G is the Greenwich ascension which can be obtained from the orbital parameters.

Furthermore, ${}^{I}\boldsymbol{x}_o$ can be calculated by

$$
{}^{I}\boldsymbol{x}_o = \boldsymbol{R}_{IO}\,{}^{O}\boldsymbol{x}_o \tag{11}
$$

where ${}^{O}\boldsymbol{x}_o = [1\ 0\ 0]^T$ and $\boldsymbol{R}_{IO}$ is the transform matrix from the Orbital Reference Frame $\boldsymbol{F}_O$ to Inertial Reference Frame $\boldsymbol{F}_I$ which can be obtained from the satellite orbital parameters. Substituting Eqs.(9)-(11) into Eq.(8), $\boldsymbol{R}_{TI}$ can be calculated. Therefore, according to the above discussion, the target quaternion, $\boldsymbol{q}_{TI} = \left[\bar{q}_{TI}\ \hat{\boldsymbol{q}}_{TI}^T\right]^T \in \mathbb{R}\times\mathbb{R}^3$, relative to $\boldsymbol{F}_I$ can also been obtained from Eq.(8).

Note that the target reference frame is not a stationary frame with respect to $\boldsymbol{F}_I$. To achieve the attitude tracking with the "PD+" technique, the angular velocity and acceleration of the target reference frame are required, which will be presented in the following sections.

B. Target angular velocity

For simplicity, we define $\boldsymbol{\rho}_1 = \|\boldsymbol{\rho}_T\|\boldsymbol{S}_{sun} + \boldsymbol{\rho}_T$ and $\boldsymbol{\rho}_2 = \boldsymbol{z}_T \times \boldsymbol{x}_o$. Then, according to Eq.7, ${}^I\boldsymbol{z}_T$ and ${}^I\boldsymbol{y}_T$ can be rewritten as

$$ {}^I\boldsymbol{z}_T = \frac{{}^I\boldsymbol{\rho}_1}{\|{}^I\boldsymbol{\rho}_1\|}, {}^I\boldsymbol{y}_T = \frac{{}^I\boldsymbol{\rho}_2}{\|{}^I\boldsymbol{\rho}_2\|} \tag{12} $$

It should be noted that the Sun is running at a very slow speed compared to the spacecraft motion and orientation. Thus, it can be approximately thought that the Sun direction vector $\boldsymbol{S}_{sun}$ is stationary with respect to the inertial reference frame, i.e. $\dot{\boldsymbol{S}}_{sun} = 0$. Moreover, for a target point on the surface of the Earth, it is apparent that $\dot{\boldsymbol{r}}_T = \boldsymbol{\omega}_E \times \boldsymbol{r}_T$ where $\boldsymbol{\omega}_E$ is the angular velocity of the Earth rotation. Thus,

$$ {}^I\dot{\boldsymbol{\rho}}_1 = \frac{{}^I\boldsymbol{\rho}_T^T\ {}^I\dot{\boldsymbol{\rho}}_T}{\|{}^I\boldsymbol{\rho}_T\|}\ {}^I\boldsymbol{S}_{sun} + {}^I\dot{\boldsymbol{\rho}}_T \tag{13} $$

where ${}^I\dot{\boldsymbol{\rho}}_T = {}^I\dot{\boldsymbol{r}}_T - {}^I\dot{\boldsymbol{r}}_s = {}^I\boldsymbol{\omega}_E \times {}^I\boldsymbol{r}_T - {}^I\boldsymbol{V}_s$ in which ${}^I\boldsymbol{V}_s$ is the speed of the satellite which can be obtained from the GPS. Furthermore, the time derivative of the $\boldsymbol{z}_T$ in the Inertial Reference Frame $\boldsymbol{F}_I$ can be calculated by

$$ {}^I\dot{\boldsymbol{z}}_T = \frac{{}^I\dot{\boldsymbol{\rho}}_1\|{}^I\boldsymbol{\rho}_1\| - {}^I\boldsymbol{\rho}_1 \frac{d\|{}^I\boldsymbol{\rho}_1\|}{dt}}{\|{}^I\boldsymbol{\rho}_1\|^2} = \frac{{}^I\dot{\boldsymbol{\rho}}_1}{\|{}^I\boldsymbol{\rho}_1\|} - \frac{{}^I\boldsymbol{\rho}_1\ {}^I\boldsymbol{\rho}_1^T\ {}^I\dot{\boldsymbol{\rho}}_1}{\|{}^I\boldsymbol{\rho}_1\|^3} = \left(\boldsymbol{E}_3 - {}^I\boldsymbol{z}_T\ {}^I\boldsymbol{z}_T^T\right)\frac{{}^I\dot{\boldsymbol{\rho}}_1}{\|{}^I\boldsymbol{\rho}_1\|} \tag{14} $$

Similarly, for $\boldsymbol{y}_T$, it can also be obtained that

$$ {}^I\dot{\boldsymbol{y}}_T = \left(\boldsymbol{E}_3 - {}^I\boldsymbol{y}_T\ {}^I\boldsymbol{y}_T^T\right)\frac{{}^I\dot{\boldsymbol{\rho}}_2}{\|{}^I\boldsymbol{\rho}_2\|} \tag{15} $$

in which ${}^I\dot{\boldsymbol{\rho}}_2 = {}^I\dot{\boldsymbol{z}}_T \times {}^I\boldsymbol{x}_o + {}^I\boldsymbol{z}_T \times {}^I\dot{\boldsymbol{x}}_o$, ${}^I\dot{\boldsymbol{x}}_o = {}^I\boldsymbol{\omega}_o \times {}^I\boldsymbol{x}_o$ and ${}^I\boldsymbol{\omega}_o$ is the orbital angular velocity of the spacecraft. In Eqs.(13)-(15), the following equality

$$ \frac{d\|\boldsymbol{\rho}\|}{dt} = \frac{d\sqrt{\boldsymbol{\rho}^T\boldsymbol{\rho}}}{dt} = \frac{\boldsymbol{\rho}^T\dot{\boldsymbol{\rho}}}{\|\boldsymbol{\rho}\|} \tag{16} $$

is applied. Furthermore, we have

$$ {}^I\dot{\boldsymbol{y}}_T = {}^I\boldsymbol{\omega}_{TI} \times {}^I\boldsymbol{y}_T, {}^I\dot{\boldsymbol{z}}_T = {}^I\boldsymbol{\omega}_{TI} \times {}^I\boldsymbol{z}_T \tag{17} $$

which will also yield that

$$
\begin{aligned}
{}^{I}\boldsymbol{y}_T \times {}^{I}\dot{\boldsymbol{y}}_T &= {}^{I}\boldsymbol{y}_T \times \left({}^{I}\boldsymbol{\omega}_{TI} \times {}^{I}\boldsymbol{y}_T \right) \\
&= \left({}^{I}\boldsymbol{y}_T \cdot {}^{I}\boldsymbol{y}_T \right) {}^{I}\boldsymbol{\omega}_{TI} - \left({}^{I}\boldsymbol{y}_T \cdot {}^{I}\boldsymbol{\omega}_{TI} \right) {}^{I}\boldsymbol{y}_T \\
&= {}^{I}\boldsymbol{\omega}_{TI} - \left({}^{I}\boldsymbol{y}_T \cdot {}^{I}\boldsymbol{\omega}_{TI} \right) {}^{I}\boldsymbol{y}_T \\
&= {}^{I}\boldsymbol{\omega}_{TI} - \frac{\left({}^{I}\boldsymbol{z}_T \times {}^{I}\boldsymbol{x}_o \right) \cdot {}^{I}\boldsymbol{\omega}_{TI}}{\| {}^{I}\boldsymbol{z}_T \times {}^{I}\boldsymbol{x}_o \|} {}^{I}\boldsymbol{y}_T \\
&= {}^{I}\boldsymbol{\omega}_{TI} - \frac{\left({}^{I}\boldsymbol{\omega}_{TI} \times {}^{I}\boldsymbol{z}_T \right) \cdot {}^{I}\boldsymbol{x}_o}{\| {}^{I}\boldsymbol{z}_T \times {}^{I}\boldsymbol{x}_o \|} {}^{I}\boldsymbol{y}_T \\
&= {}^{I}\boldsymbol{\omega}_{TI} - \frac{{}^{I}\dot{\boldsymbol{z}}_T \cdot {}^{I}\boldsymbol{x}_o}{\| {}^{I}\boldsymbol{z}_T \times {}^{I}\boldsymbol{x}_o \|} {}^{I}\boldsymbol{y}_T
\end{aligned}
\tag{18}
$$

Thus,

$$
{}^{I}\boldsymbol{\omega}_{TI} = {}^{I}\boldsymbol{y}_T \times {}^{I}\dot{\boldsymbol{y}}_T + \frac{{}^{I}\dot{\boldsymbol{z}}_T \cdot {}^{I}\boldsymbol{x}_o}{\| {}^{I}\boldsymbol{z}_T \times {}^{I}\boldsymbol{x}_o \|} {}^{I}\boldsymbol{y}_T \tag{19}
$$

Note that all vectors, including ${}^{I}\boldsymbol{y}_T$, ${}^{I}\dot{\boldsymbol{y}}_T$, ${}^{I}\boldsymbol{z}_T$, ${}^{I}\dot{\boldsymbol{z}}_T$, ${}^{I}\boldsymbol{x}_o$, are all known, indicating that the angular velocity, ${}^{I}\boldsymbol{\omega}_{TI}$, of the Target Reference Frame $\boldsymbol{F}_T$ relative to the Inertia Reference Frame $\boldsymbol{F}_I$ can be obtained.

C. Target angular acceleration

The target angular acceleration, ${}^{I}\dot{\boldsymbol{\omega}}_{TI}$, of the Target Reference Frame $\boldsymbol{F}_T$ relative to the Inertia Reference Frame $\boldsymbol{F}_I$ can be calculated by differentiating the target angular rate ${}^{I}\boldsymbol{\omega}_{TI}$.

$$
\begin{aligned}
{}^{I}\dot{\omega}_{TI} &= {}^{I}\boldsymbol{y}_T \times {}^{I}\ddot{\boldsymbol{y}}_T + \frac{{}^{I}\dot{\boldsymbol{z}}_T \cdot {}^{I}\boldsymbol{x}_o}{\| {}^{I}\boldsymbol{z}_T \times {}^{I}\boldsymbol{x}_o \|} {}^{I}\dot{\boldsymbol{y}}_T + \left(\frac{{}^{I}\ddot{\boldsymbol{z}}_T \cdot {}^{I}\boldsymbol{x}_o + {}^{I}\dot{\boldsymbol{z}}_T \cdot {}^{I}\dot{\boldsymbol{x}}_o}{\| {}^{I}\boldsymbol{z}_T \times {}^{I}\boldsymbol{x}_o \|} - \frac{\left({}^{I}\dot{\boldsymbol{z}}_T \cdot {}^{I}\boldsymbol{x}_o \right) \left({}^{I}\boldsymbol{z}_T \times {}^{I}\boldsymbol{x}_o \right)^T \left({}^{I}\dot{\boldsymbol{z}}_T \times {}^{I}\boldsymbol{x}_o + {}^{I}\boldsymbol{z}_T \times {}^{I}\dot{\boldsymbol{x}}_o \right)}{\| {}^{I}\boldsymbol{z}_T \times {}^{I}\boldsymbol{x}_o \|^3} \right) {}^{I}\boldsymbol{y}_T \\
&= {}^{I}\boldsymbol{y}_T \times {}^{I}\ddot{\boldsymbol{y}}_T + \frac{{}^{I}\dot{\boldsymbol{z}}_T \cdot {}^{I}\boldsymbol{x}_o}{\| {}^{I}\boldsymbol{z}_T \times {}^{I}\boldsymbol{x}_o \|} {}^{I}\dot{\boldsymbol{y}}_T + \left(\frac{{}^{I}\ddot{\boldsymbol{z}}_T \cdot {}^{I}\boldsymbol{x}_o + {}^{I}\dot{\boldsymbol{z}}_T \cdot \left({}^{I}\boldsymbol{\omega}_o \times {}^{I}\boldsymbol{x}_o \right)}{\| {}^{I}\boldsymbol{z}_T \times {}^{I}\boldsymbol{x}_o \|} - \frac{\left({}^{I}\dot{\boldsymbol{z}}_T \cdot {}^{I}\boldsymbol{x}_o \right) \left({}^{I}\boldsymbol{z}_T \times {}^{I}\boldsymbol{x}_o \right)^T \left({}^{I}\dot{\boldsymbol{z}}_T \times {}^{I}\boldsymbol{x}_o + {}^{I}\boldsymbol{z}_T \times \left({}^{I}\boldsymbol{\omega}_o \times {}^{I}\boldsymbol{x}_o \right) \right)}{\| {}^{I}\boldsymbol{z}_T \times {}^{I}\boldsymbol{x}_o \|^3} \right) {}^{I}\boldsymbol{y}_T
\end{aligned}
\tag{20}
$$

It is indicated from Eq.(20) that ${}^{I}\dot{\boldsymbol{\omega}}_{TI}$ can be calculated if ${}^{I}\ddot{\boldsymbol{y}}_T$ and ${}^{I}\ddot{\boldsymbol{z}}_T$ are known. From Eqs.(14) and Eq.(15), it can be obtained that

$$
{}^{I}\ddot{\boldsymbol{z}}_T = \left(\boldsymbol{E}_3 - {}^{I}\boldsymbol{z}_T \, {}^{I}\boldsymbol{z}_T^T \right) \left(\frac{{}^{I}\ddot{\boldsymbol{\rho}}_1}{\| {}^{I}\boldsymbol{\rho}_1 \|} - \frac{{}^{I}\dot{\boldsymbol{\rho}}_1 \, {}^{I}\boldsymbol{\rho}_1^T \, {}^{I}\dot{\boldsymbol{\rho}}_1}{\| {}^{I}\boldsymbol{\rho}_1 \|^3} \right) - \left({}^{I}\dot{\boldsymbol{z}}_T \, {}^{I}\boldsymbol{z}_T^T + {}^{I}\boldsymbol{z}_T \, {}^{I}\dot{\boldsymbol{z}}_T^T \right) \frac{{}^{I}\dot{\boldsymbol{\rho}}_1}{\| {}^{I}\boldsymbol{\rho}_1 \|} \tag{21}
$$

and

$$
{}^{I}\ddot{\boldsymbol{y}}_T = \left(\boldsymbol{E}_3 - {}^{I}\boldsymbol{y}_T \, {}^{I}\boldsymbol{y}_T^T \right) \left(\frac{{}^{I}\ddot{\boldsymbol{\rho}}_2}{\| {}^{I}\boldsymbol{\rho}_2 \|} - \frac{{}^{I}\dot{\boldsymbol{\rho}}_2 \, {}^{I}\boldsymbol{\rho}_2^T \, {}^{I}\dot{\boldsymbol{\rho}}_2}{\| {}^{I}\boldsymbol{\rho}_2 \|^3} \right) - \left({}^{I}\dot{\boldsymbol{y}}_T \, {}^{I}\boldsymbol{y}_T^T + {}^{I}\boldsymbol{y}_T \, {}^{I}\dot{\boldsymbol{y}}_T^T \right) \frac{{}^{I}\dot{\boldsymbol{\rho}}_2}{\| {}^{I}\boldsymbol{\rho}_2 \|} \tag{22}
$$

in which ${}^{I}\ddot{\boldsymbol{\rho}}_1$ and ${}^{I}\ddot{\boldsymbol{\rho}}_2$ are required. From Eq.(13), we know that

$$
{}^{I}\ddot{\boldsymbol{\rho}}_1 = \left(\boldsymbol{E}_3 - \frac{{}^{I}\boldsymbol{\rho}_T \, {}^{I}\boldsymbol{\rho}_T^T}{\| {}^{I}\boldsymbol{\rho}_T^2 \|} \right) \frac{{}^{I}\dot{\boldsymbol{\rho}}_T^T \, {}^{I}\dot{\boldsymbol{\rho}}_T}{\| {}^{I}\dot{\boldsymbol{\rho}}_T \|} {}^{I}\boldsymbol{S}_{sun} + \frac{{}^{I}\boldsymbol{\rho}_T^T \, {}^{I}\ddot{\boldsymbol{\rho}}_T}{\| {}^{I}\boldsymbol{\rho}_T \|} {}^{I}\boldsymbol{S}_{sun} + {}^{I}\ddot{\boldsymbol{\rho}}_T \tag{23}
$$

where ${}^I\ddot{\boldsymbol{\rho}}_T = {}^I\boldsymbol{\omega}_E \times {}^I\dot{\boldsymbol{r}}_T - {}^I\dot{\boldsymbol{V}}_s = {}^I\boldsymbol{\omega}_E \times \left({}^I\boldsymbol{\omega}_E \times {}^I\boldsymbol{r}_T\right) - {}^I\dot{\boldsymbol{V}}_s$. Similarly,

$$\begin{aligned} {}^I\ddot{\boldsymbol{\rho}}_2 &= {}^I\ddot{\boldsymbol{z}}_T \times {}^I\boldsymbol{x}_o + 2\,{}^I\dot{\boldsymbol{z}}_T \times {}^I\dot{\boldsymbol{x}}_o + {}^I\boldsymbol{z}_T \times {}^I\ddot{\boldsymbol{x}}_o \\ &= {}^I\ddot{\boldsymbol{z}}_T \times {}^I\boldsymbol{x}_o + 2\,{}^I\dot{\boldsymbol{z}}_T \times {}^I\dot{\boldsymbol{x}}_o + {}^I\boldsymbol{z}_T \times \left({}^I\boldsymbol{\omega}_o \times {}^I\dot{\boldsymbol{x}}_o\right) \\ &= {}^I\ddot{\boldsymbol{z}}_T \times {}^I\boldsymbol{x}_o + 2\,{}^I\dot{\boldsymbol{z}}_T \times {}^I\dot{\boldsymbol{x}}_o + {}^I\boldsymbol{z}_T \times \left[{}^I\boldsymbol{\omega}_o \times \left({}^I\boldsymbol{\omega}_o \times {}^I\boldsymbol{x}_o\right)\right] \end{aligned} \tag{24}$$

By substituting Eqs.(21)-(24) into Eq.(20), ${}^I\dot{\boldsymbol{\omega}}_{TI}$ can be calculated.

However, from Eqs.(19) and (20), it can be seen that the differentiation process is difficult. To simplify the calculation, we introduce another method to calculate the target angular rate $\boldsymbol{\omega}_{TI}$ and the target angular acceleration $\dot{\boldsymbol{\omega}}_{TI}$. For $\boldsymbol{\omega}_{TI}$, according to Eq.(17), it can also be rewritten as

$${}^T\dot{\boldsymbol{y}}_T = {}^T\boldsymbol{\omega}_{TI} \times {}^T\boldsymbol{y}_T,\ {}^T\dot{\boldsymbol{z}}_T = {}^T\boldsymbol{\omega}_{TI} \times {}^T\boldsymbol{z}_T \tag{25}$$

where ${}^T\boldsymbol{y}_T = [0\ 1\ 0]^T$, ${}^T\dot{\boldsymbol{y}}_T = \boldsymbol{R}_{TI}\,{}^T\dot{\boldsymbol{y}}_I$, ${}^T\boldsymbol{z}_T = [0\ 0\ 1]^T$ and ${}^T\dot{\boldsymbol{z}}_T = \boldsymbol{R}_{TI}\,{}^T\dot{\boldsymbol{z}}_I$. Thus, solving, Eq.(25), we obtain

$${}^T\boldsymbol{\omega}_{TI} = \begin{bmatrix} -{}^T\dot{\boldsymbol{z}}_T(2) & {}^T\dot{\boldsymbol{z}}_T(1) & -{}^T\dot{\boldsymbol{y}}_T(1) \end{bmatrix}^T = \begin{bmatrix} {}^T\dot{\boldsymbol{y}}_T(3) & {}^T\dot{\boldsymbol{z}}_T(1) & -{}^T\dot{\boldsymbol{y}}_T(1) \end{bmatrix}^T \tag{26}$$

Similarly, for ${}^T\dot{\boldsymbol{\omega}}_{TI}$, from Eq.(25), it can be obtained that

$$\begin{cases} {}^T\ddot{\boldsymbol{y}}_T = {}^T\dot{\boldsymbol{\omega}}_{TI} \times {}^T\boldsymbol{y}_T + {}^T\boldsymbol{\omega}_{TI} \times {}^T\dot{\boldsymbol{y}}_T \\ {}^T\ddot{\boldsymbol{z}}_T = {}^T\dot{\boldsymbol{\omega}}_{TI} \times {}^T\boldsymbol{z}_T + {}^T\boldsymbol{\omega}_{TI} \times {}^T\dot{\boldsymbol{z}}_T \end{cases} \tag{27}$$

By denoting ${}^T\boldsymbol{\mu}_y = {}^T\ddot{\boldsymbol{y}}_T - {}^T\boldsymbol{\omega}_{TI} \times {}^T\dot{\boldsymbol{y}}_T$ and ${}^T\boldsymbol{\mu}_z = {}^T\ddot{\boldsymbol{z}}_T - {}^T\boldsymbol{\omega}_{TI} \times {}^T\dot{\boldsymbol{z}}_T$, we have

$${}^T\dot{\boldsymbol{\omega}}_T = \begin{bmatrix} -{}^T\boldsymbol{\mu}_z(2) & {}^T\boldsymbol{\mu}_z(1) & -{}^T\boldsymbol{\mu}_y(1) \end{bmatrix}^T = \begin{bmatrix} {}^T\boldsymbol{\mu}_y(3) & {}^T\boldsymbol{\mu}_z(1) & -{}^T\boldsymbol{\mu}_y(1) \end{bmatrix}^T \tag{28}$$

where ${}^T\ddot{\boldsymbol{y}}_T = \boldsymbol{R}_{TI}\,{}^I\ddot{\boldsymbol{y}}_T$ and ${}^T\ddot{\boldsymbol{z}}_T = \boldsymbol{R}_{TI}\,{}^I\ddot{\boldsymbol{z}}_T$. ${}^T\ddot{\boldsymbol{y}}_I$ and ${}^T\ddot{\boldsymbol{z}}_I$ can be obtained from Eqs.(22) and (21).

D. Discussion

1. The condition to achieve the sunlight-reflected staring

In previous sections, the target quaternion, angular velocity and angular acceleration of the target reference frame have been given, as the target attitude to be tracked such that the reflected sunlight can point to the target point O_T. However, not every selected target point can not be starred by the reflected sunlight all the time. As a simple example, when the spacecraft is running into the shadow area, the sunlight cannot be reflected

by the spacecraft. So the mission cannot be achieved in this situation. What follows will give some analysis about the conditions under which the sunlight-reflected staring can be achieved. The following analysis is presented based on the Earth globular hypothesis for simplicity.

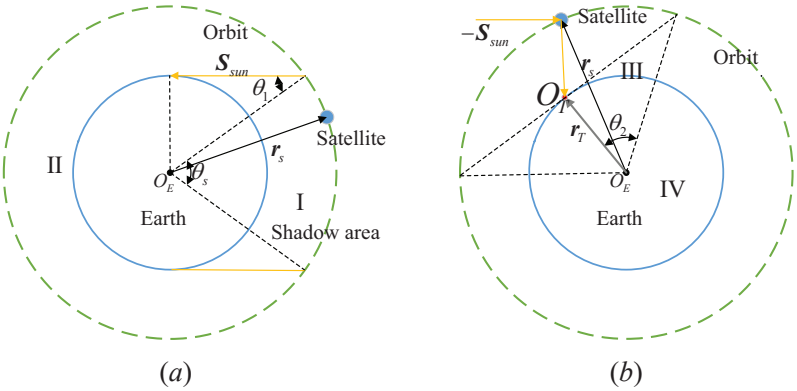

Fig. 4 Sun-reflected staring condition analysis

Firstly, as it is shown in Fig.(4(a)), when the spacecraft is running in Region I (shadow area), it cannot receive the sunlight. In other words, the sun-reflected staring can be achieved only when the spacecraft is in Region II as described in Fig.(4(a)). Mathematically, it follows that

$$\arccos\left(\frac{\boldsymbol{r}_s \cdot (-\boldsymbol{S}_{sun})}{\|\boldsymbol{r}_s\|}\right) \geq \theta_1 = \arcsin\frac{R_E}{R_E + R_h} \tag{29}$$

where R_h is the orbital height (from the surface to the mass center of the spacecraft) and R_E is the Earth radius. On the other hand, as described in Fig.(4(b)), if the spacecraft is running in Region IV, the satellite-target vector, $\boldsymbol{\rho}_T$ will pass through the Earth, indicating that the reflected sunlight will be occluded by the Earth and the reflected sunlight cannot reach the target point. That is to say, mathematically,

$$\frac{\boldsymbol{r}_s \cdot \boldsymbol{r}_T}{\|\boldsymbol{r}_s\|\|\boldsymbol{r}_T\|} \geq \cos\theta_2 = \frac{R_E}{R_E + R_h} \tag{30}$$

Therefore, from the previous discussion, it can be concluded that the necessary condition when the reflected staring task can be achieved is that

$$\boldsymbol{r}_s \in \{\boldsymbol{r}_s \in \mathbb{R}^3 : \arccos\left(\frac{\boldsymbol{r}_s \cdot (-\boldsymbol{S}_{sun})}{\|\boldsymbol{r}_s\|}\right) \geq \arcsin\frac{R_E}{R_E + R_h}, and \frac{\boldsymbol{r}_s \cdot \boldsymbol{r}_T}{\|\boldsymbol{r}_s\|\|\boldsymbol{r}_T\|} \geq \frac{R_E}{R_E + R_h}\} \tag{31}$$

The previous condition can help to determine when we can start and end the task. Furthermore, according to Eq.(31), if T denote the orbital period, it can be calculated approximately that the longest time the sunlight-reflection staring can last is $\theta_2 T/\pi$. For example, for an orbit whose height is $500\,\mathrm{km}$, $T = 5677$ seconds and $\theta_2 = 0.3878\,\mathrm{rad}$, it yields that the longest time of the staring is 700 seconds.

2. *The actual longitude and latitude calculation of the staring point*

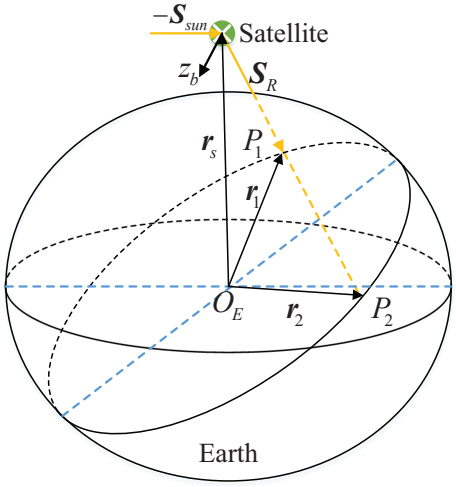

Fig. 5 The actual staring point calculation

So far, the target attitude and the conditions to achieve the sunlight-reflection staring have been obtained. What follows will discuss how to calculate the geographic longitude and latitude of the actual staring point. As presented in Fig.(5), P_1 and P_2 will correspond to the same target attitude. However, only P_1 can be an effective target point whereas P_2 will be blocked. That is to say, the reflected sunlight, denoted by $\boldsymbol{S}_R$, will point to P_1 on the Earth surface, instead of P_2. In this case, P_1 is called actual staring point while P_2 is the virtual staring point. Then the reflected sunlight can be described by

$$\boldsymbol{S}_R = (z_b - \boldsymbol{S}_{sun}) / \|z_b - \boldsymbol{S}_{sun}\| \tag{32}$$

with $\|\boldsymbol{S}_R\| = 1$ and then it can be obtained that

$$\boldsymbol{r}_1 = \boldsymbol{r}_s + r_R \boldsymbol{S}_R \tag{33}$$

where r_R is a positive real number to be determined.

To simplify the problem, we first assume that the Earth is spherical. Based on the assumption above and because the target point should be on the Earth surface, it is known that $\|\boldsymbol{r}_1\| = R_E$ is the Earth radius.

Therefore, we have

$$r_R^2 + 2\zeta_1 r_R + \zeta_2 = 0 \tag{34}$$

in which $\zeta_1 = \boldsymbol{S}_R \cdot \boldsymbol{r}_s$ and $\zeta_2 = \|r_s\|^2 - R_E^2 > 0$. if the solution of Eq.(34) does not exist, $\zeta_1^2 - \zeta_2 < 0$, the reflected sunlight will not reach to any point on the Earth surface. Otherwise, two solutions of Eq.(34) can be given by

$$r_{R1} = -\zeta_1 + \sqrt{\zeta_1^2 - \zeta_2}, r_{R2} = -\zeta_1 - \sqrt{\zeta_1^2 - \zeta_2} \tag{35}$$

To guarantee r_R to be a real positive number, the following conditions should be satisfied,

$$\zeta_1 < 0, \zeta_1^2 > \zeta_2 \tag{36}$$

which is equivalent to $\cos < \boldsymbol{r}_s, \boldsymbol{S}_R > < -\sqrt{\left(R_h^2 + 2R_h R_E\right) / \left(R_h + R_E\right)^2}$. Once Eq.(36) holds, the two solutions of Eq.(34) will be positive real numbers and the vector from the Earth center to the staring point can be described by

$$\boldsymbol{r}_1 = \boldsymbol{r}_s + r_{R2}\boldsymbol{S}_R \tag{37}$$

and the latitude and longitude can be then calculated. However, the Earth is not a sphere. It is usually assumed that the Earth is a body of revolution represented by an ellipsoid rotating around its minor-axis. Based on this assumption, the meridian plane of the Earth is regarded as an ellipsoid with the major axis R_E and minor axis R_P and the equatorial plane is regarded as a circle with radius R_E. Thus, for any point on the Earth's surface, the following constraint on its position vector in $\boldsymbol{F}_E$ exists:

$$\frac{x^2}{R_E^2} + \frac{y^2}{R_E^2} + \frac{z^2}{R_P^2} = 1 \tag{38}$$

To calculate the intersection of the reflected sunlight and the Earth surface, a linear operator $\boldsymbol{M} : \mathbb{R}^3 \to \mathbb{R}^3$ is introduced acting on $\boldsymbol{r}_1 = [x\ y\ z]^T$ as follows:

$$\boldsymbol{M}\left(\boldsymbol{r}_1\right) = diag([1/R_E\ 1/R_E\ 1/R_P])\boldsymbol{r}_1 \tag{39}$$

Thus, for any vector from the Earth center to the point on the Earth surface, $\boldsymbol{r}_1 = [x\ y\ z]^T$, we have, according to Eq.(38), $\|\boldsymbol{M}\left(\boldsymbol{r}_1\right)\| = 1$. On this basis, Eq.(33) can be rewritten as

$$\boldsymbol{M}(\boldsymbol{r}_1) = \boldsymbol{M}(\boldsymbol{r}_s) + r_R\boldsymbol{M}(\boldsymbol{S}_R) \tag{40}$$

and we can still have the equation similar to Eq.(34), where $\zeta_1 = \boldsymbol{r}_s^T \boldsymbol{M}^T \boldsymbol{M}\boldsymbol{S}_R / \|\boldsymbol{M}\boldsymbol{S}_R\|^2$ and $\zeta_2 = \left(\|\boldsymbol{M}\boldsymbol{r}_s\|^2 - 1\right) / \|\boldsymbol{M}\boldsymbol{S}_R\|^2$. Thus, we can perform a similar discussion to the previous one to solve the solution of Eq.(37) to obtain r_{R1} and r_{R2} and then, the latitude and longitude of the staring point can be calculated.

IV. Control law formulation

In this section, we will present a control law for the spacecraft to track the target attitude given in Section III. To propose the tracking control law, the relative attitude of the spacecraft with respect to the Target Reference Frame $\boldsymbol{F}_T$ can be demonstrated by

$$\boldsymbol{q}_{BT} = \boldsymbol{q}_{TI}^* \otimes \boldsymbol{q}_{BI} \tag{41}$$

$$^B\boldsymbol{\omega}_{BT} = {}^B\boldsymbol{\omega}_{BI} - \boldsymbol{R}_{BT}\, {}^T\boldsymbol{\omega}_{TI} \tag{42}$$

where $\boldsymbol{R}_{BT}$ is the transform matrix from $\boldsymbol{F}_T$ to $\boldsymbol{F}_B$ which can be described as

$$\boldsymbol{R}_{BT} = \left(\bar{q}_{BT}^2 - \hat{\boldsymbol{q}}_{BT}^T \hat{\boldsymbol{q}}_{BT}\right) \boldsymbol{E}_3 + 2\hat{\boldsymbol{q}}_{BT}\hat{\boldsymbol{q}}_{BT}^T - 2\bar{q}_{BT}\hat{\boldsymbol{q}}_{BT}^{\times} \tag{43}$$

Thus, the dynamics with regards to the relative attitude can be presented as

$$\begin{cases} \dot{\bar{q}}_{BT} = -\frac{1}{2}\hat{\boldsymbol{q}}_{BT}^T\, {}^B\boldsymbol{\omega}_{BT} \\ \dot{\hat{\boldsymbol{q}}}_{BT} = \frac{1}{2}\left(\bar{q}_{BT}\boldsymbol{E}_3 + \hat{\boldsymbol{q}}_{BT}^{\times}\right) {}^B\boldsymbol{\omega}_{BT} \end{cases} \tag{44}$$

$$\boldsymbol{I}_b\, {}^B\dot{\boldsymbol{\omega}}_{BT} = -{}^B\boldsymbol{\omega}_{BI}^{\times}\boldsymbol{I}_b\, {}^B\boldsymbol{\omega}_{BI} + \boldsymbol{I}_b\, {}^B\boldsymbol{\omega}_{BT}^{\times}\boldsymbol{R}_{BT}\, {}^T\boldsymbol{\omega}_{TI} - \boldsymbol{I}_b\boldsymbol{R}_{BT}\, {}^T\dot{\boldsymbol{\omega}}_{TI} + \boldsymbol{T}_c \tag{45}$$

To achieve the attitude tracking, similar to [18], the "PD+" control algorithm is adopted as

$$\boldsymbol{T}_c = -k_p\boldsymbol{I}_b\hat{\boldsymbol{q}}_{BT} - k_d\boldsymbol{I}_b\, {}^B\boldsymbol{\omega}_{BT} + {}^B\boldsymbol{\omega}_{BI}^{\times}\boldsymbol{I}_b\, {}^B\boldsymbol{\omega}_{BI} - \boldsymbol{I}_b\, {}^B\boldsymbol{\omega}_{BT}^{\times}\boldsymbol{R}_{BT}\, {}^T\dot{\boldsymbol{\omega}}_{TI} + \boldsymbol{I}_b\boldsymbol{R}_{BT}\, {}^T\dot{\boldsymbol{\omega}}_{TI} \tag{46}$$

where $k_p, k_d > 0$ are two control parameters to be selected. Substituting the control law of Eq.(46) into the dynamics of Eq.(45), it can be further obtained that

$$^B\dot{\boldsymbol{\omega}}_{BT} = -k_p\hat{\boldsymbol{q}}_{BT} - k_d\, {}^B\boldsymbol{\omega}_{BT} \tag{47}$$

To analyse the stability of the system, a Lyapunov function candidate is selected as

$$V = \frac{1}{2}\| {}^{B}\boldsymbol{\omega}_{BT}\|^2 + 2k_p\left(1-\bar{q}_{BT}\right) \tag{48}$$

whose time derivation along the system trajectory can be given as

$$\begin{aligned}\dot{V} &= {}^{B}\boldsymbol{\omega}_{BT}^{T}\ {}^{B}\dot{\boldsymbol{\omega}}_{BT} - k_p\hat{\boldsymbol{q}}_{BT}^{T}\ {}^{B}\boldsymbol{\omega}_{BT} \\ &= -k_d\| {}^{B}\boldsymbol{\omega}_{BT}\|^2 \le 0\end{aligned} \tag{49}$$

which implies, according to Lyapunov stability theorem [22], that the system is stable. Furthermore, $\dot{V}=0$ will lead to ${}^{B}\boldsymbol{\omega}_{BT}=0$ and ${}^{B}\dot{\boldsymbol{\omega}}_{BT}=0$, which further yields that $\hat{\boldsymbol{q}}_{BT}=0$ according to Eq. (47). Thus, by the Lasalle's theorem, the global asymptotical stability of the system can be concluded.

Remark 1 *An unit quaternion is a four-elements parameter to describe the relative attitude of the spacecraft and* $\boldsymbol{q}$ *and* $-\boldsymbol{q}$ *correspond to the same attitude. Generally, both* $[1\ 0\ 0\ 0]^T$ *and* $[-1\ 0\ 0\ 0]^T$ *can be equilibrium points of the system. In this paper,* $[1\ 0\ 0\ 0]^T$ *is set to be the stable equilibrium of the system. Furthermore, when the tracking error quaternion is stabilized to a small neighbor of the equilibrium, i.e.* $\hat{\boldsymbol{q}}_{BT}\approx 0$ *and* $\bar{q}_{BT}\approx 1$*, the error quaternion kinematics Eq.(44) can be rewritten as*

$${}^{B}\boldsymbol{\omega}_{BT} = 2\dot{\hat{\boldsymbol{q}}}_{BT} \tag{50}$$

Substituting Eq.(50) into Eq.(47), we have

$$\ddot{\hat{\boldsymbol{q}}}_{BT} + k_d\dot{\hat{\boldsymbol{q}}}_{BT} + \frac{1}{2}k_p\hat{\boldsymbol{q}}_{BT} = 0 \tag{51}$$

To guarantee a good performance of the second-order linear system, the control parameters k_p *and* k_d *are selected by* $k_d = 2\xi\omega_n$ *and* $k_p = 2\omega_n^2$ *where* ω_n *and* ξ *are respectively the frequency and damp ratio of the system to be selected. Usually,* ξ *is set to be* $\xi = 0.707$.

Remark 2 *The proposed method can be treated as an extension of the attitude staring mode of the video satellite by setting* $\boldsymbol{S}_{sun} = [0\ 0\ 0]^T$.

V. Numerical simulation

To demonstrate the effectiveness and performance of the proposed controller, a numerical simulation is conducted for a rigid spacecraft, running in a Sun-synchronous orbit, whose information is presented in

Table.1, in this section. The inertia matrix of the satellite is assumed to be

$$\boldsymbol{I}_b = \begin{bmatrix} 3.8 & 0.3 & -0.2 \\ 0.3 & 4.6 & 0.1 \\ -0.2 & 0.1 & 7.0 \end{bmatrix} \left(\mathrm{kg}\cdot\mathrm{m}^2\right).$$

The initial values of the quaternion and the angular velocity of the satellite are as follows,

$$\boldsymbol{q}_{BI}(0) = \begin{bmatrix} 0.8 & 0.4 & -0.2 & 0.4 \end{bmatrix}$$

$${}^{B}\boldsymbol{\omega}_{BI} = \begin{bmatrix} 0.0573 & 0.156 & -0.0573 \end{bmatrix} (\mathrm{deg/s})$$

It is assumed that the reaction wheels (RWs) are aligned to provide the torque here with the distribution matrix $\boldsymbol{C}_w$ which is given by

$$\boldsymbol{C}_w = \begin{bmatrix} 1 & 0 & 0 & 1/\sqrt{3} \\ 0 & 1 & 0 & 1/\sqrt{3} \\ 0 & 0 & 1 & 1/\sqrt{3} \end{bmatrix}.$$

The torque distribution method in [19] is adopted to keep energy balance and avoid wheel saturation. The control torque vector by each RW is denoted by $\boldsymbol{T}_w$, with the maximum value $0.015\,\mathrm{N}\cdot\mathrm{m}$.

Table 1 The orbital elements of the spacecraft

Orbital Elements	Value	Orbital Elements	Value
Orbital inclination(deg)	97.63	Orbital Semi-major axis(km)	6918
Orbital eccentricity	0	right ascension(deg)	338.038
Argument of perigee(deg)	0	Argument of latitude(deg)	180

Moreover, the Sun direction vector is ${}^{I}\boldsymbol{S}_{sun} = [-0.9822 \ -0.1724 \ -0.0748]^T$, which is assumed to be invariant as previously mentioned, according to the orbital information. To verify the effectiveness of the algorithm, two target points, P_1 and P_2, on the Earth surface will be selected, whose latitude and longitude are listed in Table.2. The control parameters given in Eq.(46), k_p and k_d, are selected as $k_p = 0.02, k_d = 0.142$ ($\omega_n = 0.1, k_d = 0.71$).

The target point P_1 is near to sub-satellite point of the initial time of the simulation process while P_2 is not. Therefore, it can be guessed that the reflected light will point to P_1 while P_2 will be the virtual staring

Table 2 The latitude and longitude of the target point

Target Points	Latitude $\Phi_T(\mathrm{deg})$	Longitude $\Lambda_T(\mathrm{deg})$
P_1	108E	0
P_2	108W	0

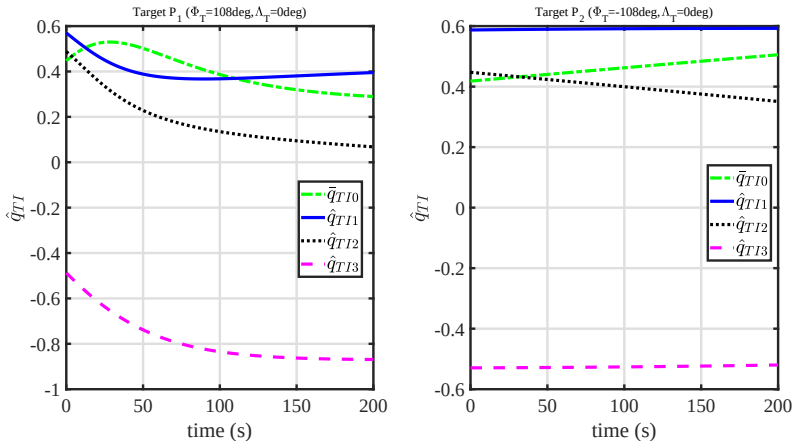

Fig. 6 The target quaternion relative to ECIRF

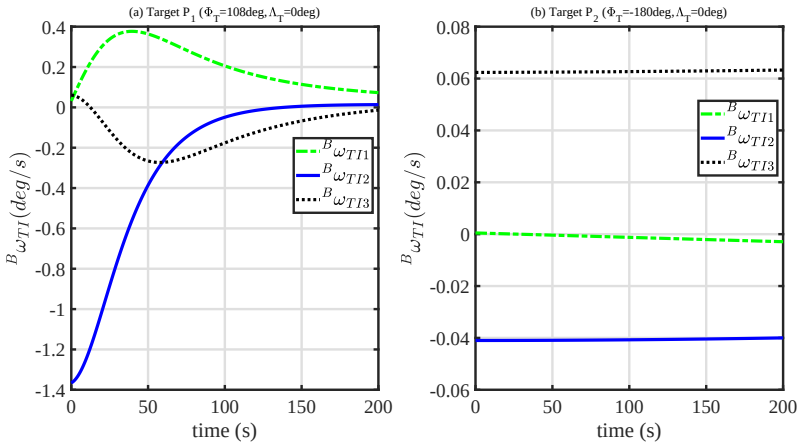

Fig. 7 The target angular rate relative to ECIRF

point due to the occlusion of the Earth. Also, to verify the control performance, the angle of the target reflected sunlight and the actual one, denoted by θ is given in the simulation. That is

$$\theta = \arccos\left(\frac{\boldsymbol{S}_R \cdot \boldsymbol{\rho}_T}{\|\boldsymbol{\rho}_T\|}\right)$$

Figs.6-7 show the target quaternion and the angular rate of $\boldsymbol{F}_T$ relative to $\boldsymbol{F}_I$. Figs.8-16 describe the control performance. It can be seen, from Figs.8-9, that for the two selected targets P_1 and P_2, the tracking

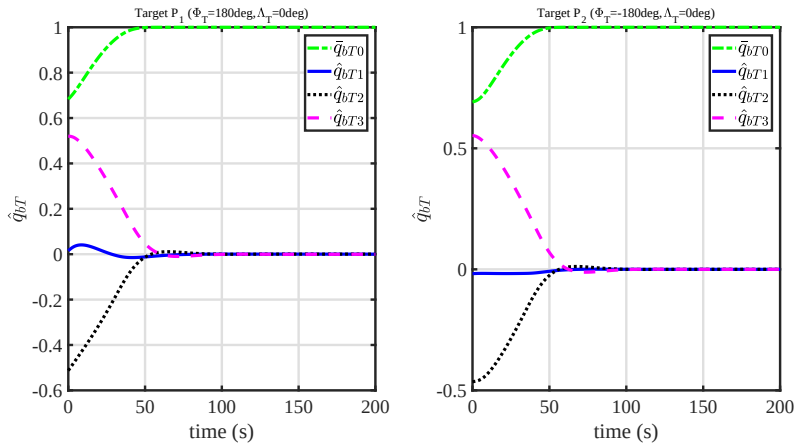

Fig. 8 The quaternion of the spacecraft relative to the target reference frame

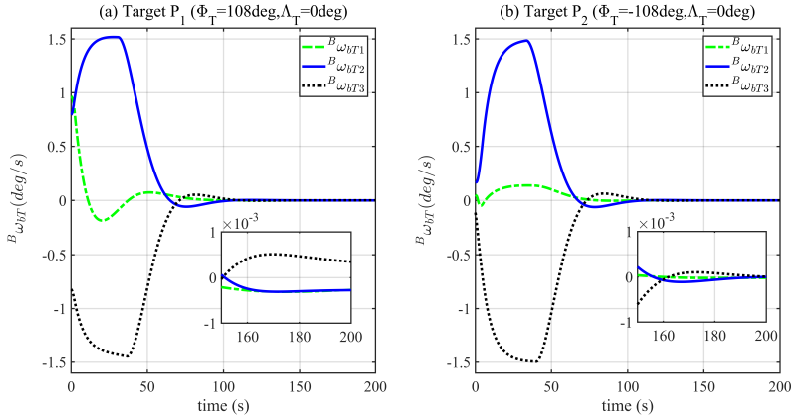

Fig. 9 The angular rate of the spacecraft relative to the target reference frame

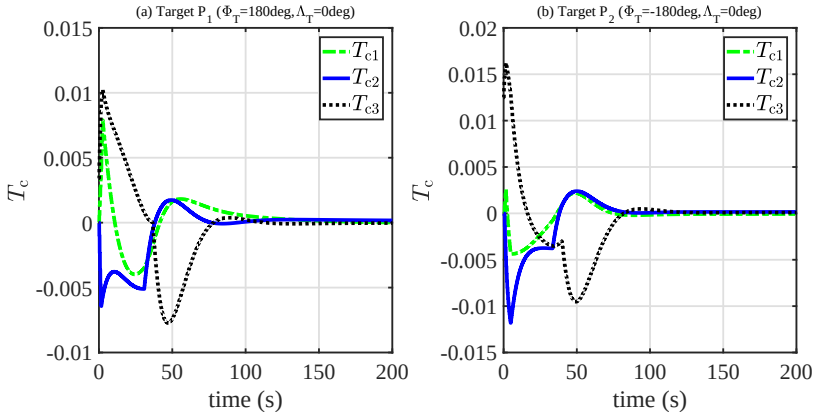

Fig. 10 The control torque of the spacecraft

error quaternion $\boldsymbol{q}_{BT}$ and the angular rate ${}^{B}\boldsymbol{\omega}_{BT}$ will converge to the equilibrium $[1\ 0\ 0\ 0]^T$ and zero,

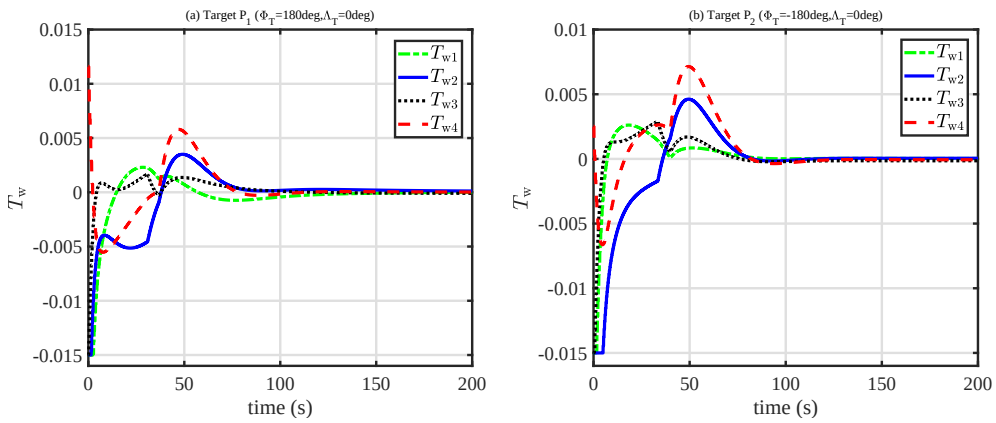

Fig. 11 The control torque provided by each RW

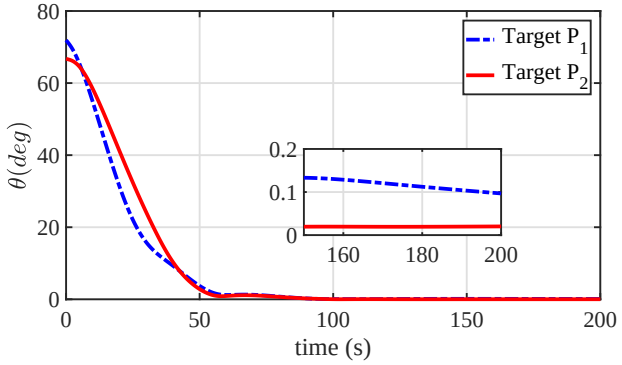

Fig. 12 The angle of the actual and target reflected sunlights

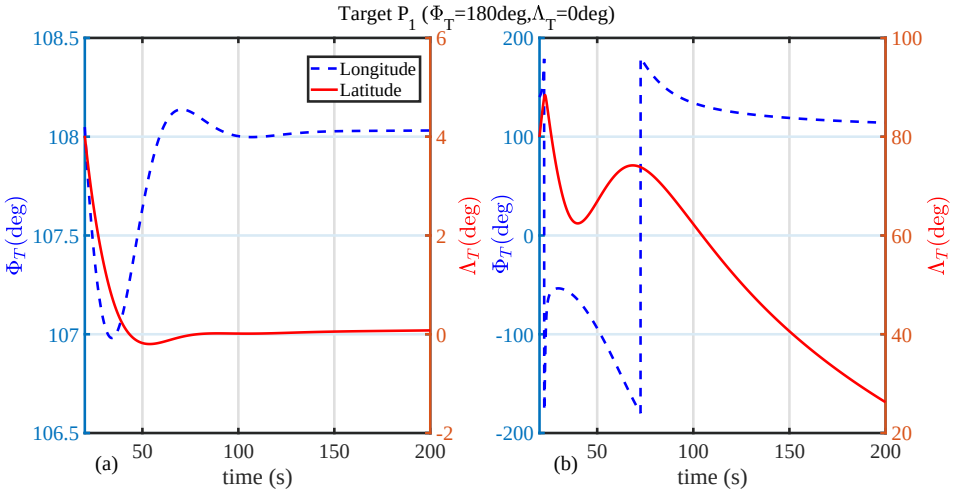

Fig. 13 The time histories of the longitude and latitude of the staring points for P_1.

respectively. The steady errors of the angular rate can reach to 10^{-3} deg/s for these two cases from the enlarged figures of Fig.9. Fig.10 shows the three-axis control torque of the spacecraft and Fig.11 is the time

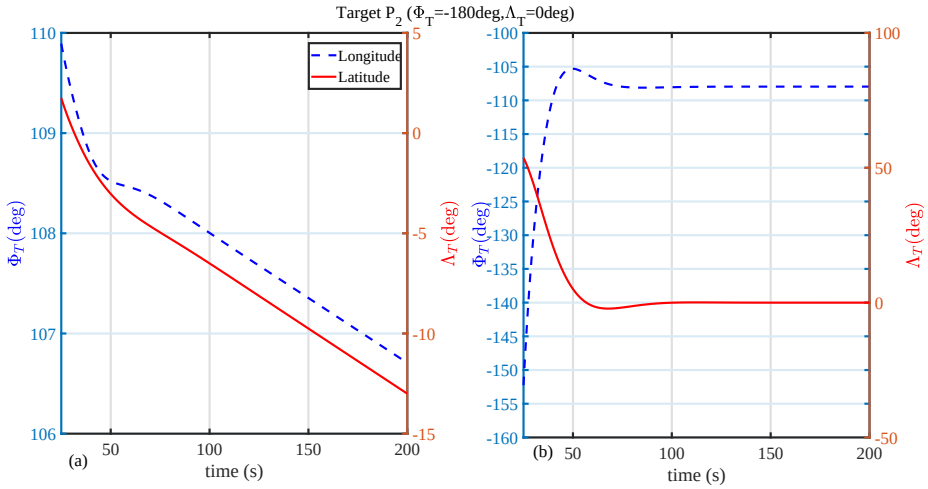

Fig. 14 The time histories of the longitude and latitude of the staring points for P_2.

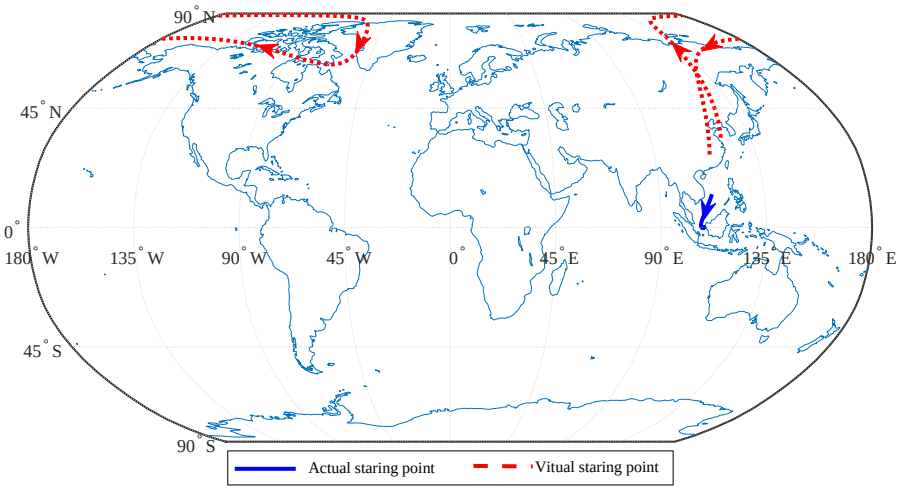

Fig. 15 The trajectories of the actual and virtual staring points for target point P_1

history of the control torque provided by each RW with the maximum output $0.015\,\mathrm{N}\cdot\mathrm{m}$. The angle of the actual reflected sunlight $\boldsymbol{S}_R$ and the satellite-target vector, $\boldsymbol{\rho}_T$ are illustrated in Fig.12, which indicates that the steady error of θ will be within $0.15\,\mathrm{deg}$ after 150 seconds. That is to say, the actual staring point may deviate from the target point by $1.42\,\mathrm{km}$, approximately.

Figs.13 and 14 show the time histories of latitude and longitude the actual and virtual staring points for these two cases in which the left figure is for the actual staring point and the right one corresponds to the the virtual staring point (occluded by the Earth). From Fig.13, it can be seen that the reflected sunlight will point to a region near the target point with the control accuracy within $0.1\,\mathrm{deg}$ in the direction of longitude

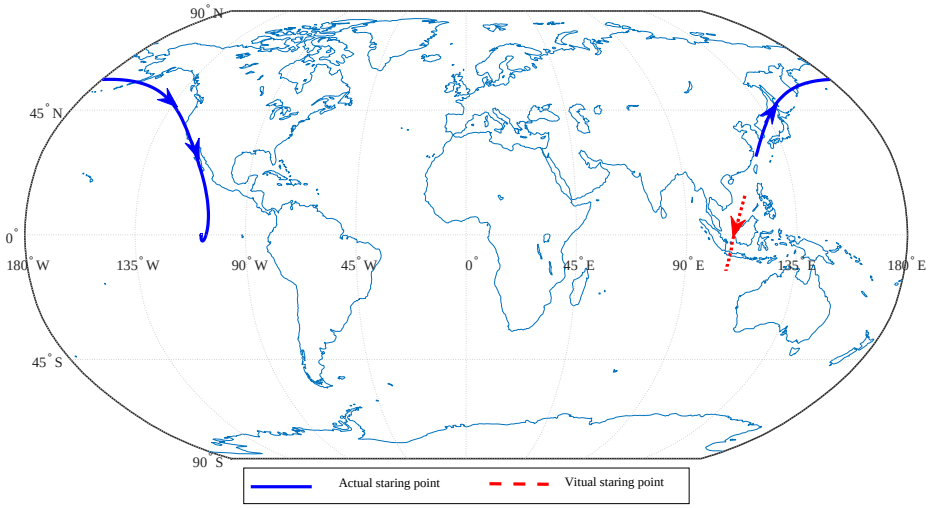

Fig. 16 The trajectories of the actual and virtual staring points for target point P_2

and latitude. Conversely, if P_2 is selected the target point, as is presented in 14, the reflected sunlight will not point to P_2 due to the occlusion of the Earth, even though the attitude tacking can still be achieved and the angle between $\boldsymbol{S}_R$ and $\boldsymbol{\rho}_T$. This phenomenon can also been found in Figs.15 and 16, which show the trajectories of the actual and virtual staring points of the reflected sunlight for these two cases.

VI. Conclusion

The attitude control problem of the spacecraft, which is performing sunlight-reflection staring operation, is discussed, such that the sunlight can point to a target point on Earth surface with the reflection of the spacecraft. A target reference frame is established firstly according to the geographic information of the selected target point. The target attitude including quaternion, angular rate and acceleration of the target reference frame are calculated later. With the help of the "PD+" control scheme, the attitude tracking can be achieved. The conditions under which the staring can be achieved are discussed followed by the calculation of the geographic latitude and longitude of the actual staring point , assuming that the Earth is an ellipsoid, which can help to determine when starting and ending this mode.

Acknowledgments

This research was supported by the Academic Excellent Foundation of BUAA for PhD Students, the National Natural Science Foundation of China (11702010) and the Fundamental Research Funds for the

Central Universities(YWF-19-BJ-J-272).

References

[1] M. Steckling, U. Renner, and H.-P. Röser, Acta Astronautica **39**, 951 (1996).

[2] S. Roemer and U. Renner, Acta Astronautica **52**, 733 (2003).

[3] R. Triharjanto, W. Hasbi, A. Widipaminto, M. Mukhayadi, and U. Renner, in *Small Satellites, Systems and Services* (2004), pp. 1–7.

[4] X. Chen, W. Steyn, and Y. Hashida, in *AIAA Guidance, Navigation, and Control Conference and Exhibit* (American Institute of Aeronautics and Astronautics, Dever,CO,U.S.A., 2000).

[5] H. Liang, Z. Sun, and X. Wu, in *2009 International Conference on Mechatronics and Automation* (2009), pp. 762–766, ISSN 2152-7431.

[6] S. N. Wu, X. Y. Sun, Z. W. Sun, and X. D. Wu, Proceedings of the Institution of Mechanical Engineers, Part G: Journal of Aerospace Engineering **224**, 215 (2010).

[7] Y. Lian, Y. Gao, and G. Zeng, Journal of Guidance, Control, and Dynamics **40**, 1278 (2017).

[8] Y. Xia, Z. Zhu, M. Fu, and S. Wang, IEEE Transactions on Industrial Electronics **58**, 647 (2011), ISSN 0278-0046.

[9] P. M. Tiwari, S. Janardhanan, and M. un Nabi, IFAC Proceedings Volumes **47**, 263 (2014), ISSN 1474-6670, 3rd International Conference on Advances in Control and Optimization of Dynamical Systems (2014), URL `http://www.sciencedirect.com/science/article/pii/S1474667016326660`.

[10] S.-C. Lo and Y.-P. Chen, Journal of Guidance, Control, and Dynamics **18**, 1345 (1995).

[11] A. Zou, K. D. Kumar, Z.-G. Hou, and X. Liu, IEEE Transactions on Systems, Man, and Cybernetics, Part B (Cybernetics) **41**, 950 (2011), ISSN 1083-4419.

[12] Y. rong Zhou and W. Huo, in *2009 IEEE International Conference on Intelligent Computing and Intelligent Systems* (2009), vol. 2, pp. 510–516.

[13] X. Huang, Q. Wang, and C. Dong, in *2009 IEEE International Conference on Intelligent Computing and Intelligent Systems* (2009), vol. 2, pp. 747–751.

[14] A. R. Fazlyab, F. F. Saberi, and M. Kabganian, Advances in Space Research **57**, 367 (2016).

[15] H. Gui and G. Vukovich, Journal of the Franklin Institute **352**, 5832 (2015).

[16] H. Gui and G. Vukovich, International Journal of Robust and Nonlinear Control **27**, 3174 (2017).

[17] Q. Hu, B. Li, and J. Qi, Aerospace Science and Technology **39**, 13 (2014).

[18] S. Song, B. Zhang, X. Wei, and X. Chen, in *2010 8th World Congress on Intelligent Control and Automation* (2010), pp. 3908–3913.

[19] Y.-h. JIA and S.-j. XU, Chinese Journal of Aeronautics **18**, 1 (2005).

[20] C. Li and M. He, in *2015 IEEE China Summit and International Conference on Signal and Information Processing (ChinaSIP)* (2015), pp. 630–634.

[21] J. Zhang, Z. Yu, and P. Xiao, in *2016 IEEE International Geoscience and Remote Sensing Symposium (IGARSS)* (2016), pp. 1106–1109, ISSN 2153-7003.

[22] H. K. Khalil and J. W. Grizzle, *Nonlinear systems*, vol. 3 (Prentice hall Upper Saddle River, NJ, 2002).